LA-UR- 96: 3712

CONF-961002--6

Title: **MATERIALS PROCESSING WITH INTENSE PULSED ION BEAMS**

Author(s): D. J. REJ, H. A. DAVIS, J. C. OLSON, G. E. REMNEV, A. N. ZAKOUTAEV, V. A. RYZHKOV, V. K. STRUTS, I. F. ISAKOV, V. A. SHULOV, N. A. NOCHEVNAYA, R. W. STINNETT, E. L. NEAU, K. YATSUI, W. JIANG

Submitted to: *Invited Talk VM-TuM7: 43rd National Symposium of the American Vacuum Society, Philadelphia October 14-18, 1996*

Journal of Vacuum Science and Technology

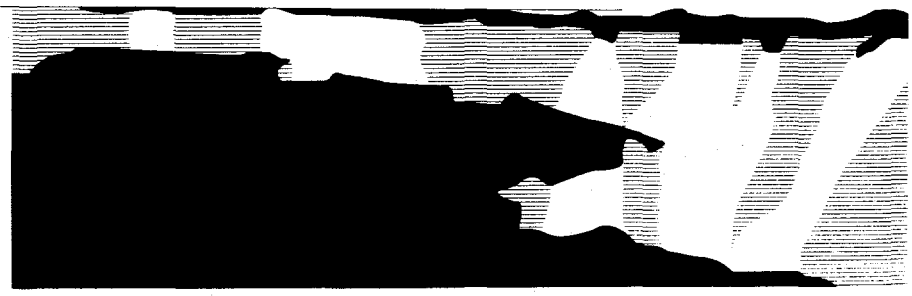

Los Alamos
NATIONAL LABORATORY

Form No. 836 R5
ST 2629 10/91

MATERIALS PROCESSING WITH INTENSE PULSED ION BEAMS

D. J. Rej, H. A. Davis and J. C. Olson*

Los Alamos National Laboratory, MS-D434, Los Alamos NM 87545

G. E. Remnev, A. N. Zakoutaev, V. A. Ryzhkov, V. K. Struts and I. F. Isakov

Nuclear Physics Institute, 2a Lenin Ave., Tomsk 634050, Russia

V. A. Shulov and N. A. Nochevnaya

Moscow Aviation Institute, Volokolamskoe sh. 4, Moscow 125871 Russia

R. W. Stinnett and E. L. Neau

QM Technologies, Inc., 3701 Hawkins NE, Albuquerque, NM 87109

K. Yatsui and W. Jiang

Nagaoka Univ. of Technology, Beam Technology Laboratory, Nagaoka, Niigata 940-21 Japan

ABSTRACT

We review research investigating the application of intense pulsed ion beams (IPIBs) for the surface treatment and coating of materials. The short range (0.1-10 μm) and high-energy density (1-50 J/cm^2) of these short-pulsed (≤ 1 μs) beams (with ion currents I = 5 - 50 kA, and energies E = 100 - 1000 keV) make them ideal to flash-heat a target surface, similar to the more familiar pulsed laser processes. IPIB surface treatment induces rapid melt and solidification at up to 10^{10} K/s to cause amorphous layer formation and the production of non-equilibrium micro-structures. At higher energy density the target surface is vaporized, and the ablated vapor is condensed as coatings onto adjacent substrates or as nanophase powders. Progress towards the development of robust, high-repetition rate IPIB accelerators is presented along with economic estimates for the cost of ownership of this technology.

I. INTRODUCTION

Intense pulsed ion beams (IPIBs) are an emerging technology that has been developed throughout the world over the last two decades primarily for nuclear fusion and high-energy density physics research.[1] IPIBs are usually created in magnetically-insulated vacuum diodes[2] from which 10 to 1000 kA beams of low-Z ions are accelerated to energies typically between 10 keV and 10 MeV in 10 to 1000 ns pulses. A typical diode (Fig. 1) requires an ion source, an accelerating voltage, and a magnetic field transverse to the acceleration gap to suppress electron flow and enhance the ion flow. Ion currents typically exceed the vacuum space-charge limit by 5-50 times owing to electrons confined in the acceleration region by the applied magnetic field. Beams are accelerated, extracted, focused, and propagated over distances of order 1 meter in a vacuum that can exceed 10^{-4} Torr. Further details of IPIB operation are described in Sec. IIIa.

IPIBs have also proven to be unique pulsed energy sources for the surface modification of materials. The shallow range (0.1-10 μm) and high energy density (1-50 J/cm^2) of these short-pulsed beams make them ideal flash-heat sources to rapidly melt or vaporize the near surface layer of targets similar to the more familiar surface treatment or deposition with pulsed lasers or electron beams. For example, direct deposition of an IPIB into the top 1 to 10 μm of a solid surface results in a rapid melt and resolidification with heating and cooling rates of up to 10^{10} K/s. These rates are sufficiently high to promote mixing, rapid diffusion, and the formation of nanocrystalline or amorphous surface layers.

An advantage of this approach over laser processing is that an IPIB delivers 0.1-10 kJ of ions per pulse to a target at an overall electrical efficiency (*i.e.*, the ratio of extracted ion beam energy to the total energy consumed in generating the beam) of 15-40% (compared to < 1% for the excimer lasers often used for similar applications). Consequently, IPIB hardware can be compact and require relatively low capital investment (see Sec. IV). This opens the promise of environmentally-conscious, low-cost, high-throughput manufacturing. Furthermore, efficient beam transport to the target and excellent coupling of incident ion energy to targets are achieved, as opposed to lasers that may have limited coupling to reflective materials or produce reflecting

plasmas at high incident fluence. The ion range is adjustable through selection of the ion species and kinetic energy. The beam energy density can be tailored through control of the beam cross-sectional area at the target to melt (at energy fluences q = 1-10 J/cm^2) or to vaporize (q = 10-50 J/cm^2) the target surface. Beam pulse duration is short ($\leq$ 1μs) to minimize thermal conduction into the target. Some disadvantages of IPIB processing over laser processing include the need to form and propagate the beams in vacuum, and the need for shielding of x-rays which are produced by relatively low-level electron currents also present in IPIB accelerators. An IPIB cannot be as tightly focused onto targets as lasers making it unsuitable for applications requiring treatment on small spatial scales. When compared with a high-power electron beams, the IPIB is advantageous in that more energy can be provided in a single pulse and that there is no need for a background plasma and magnetic field for the successful propagation of the beam. Disadvantageous with respect to electrons include higher operational voltages for a given target deposition profile and the need for an ion source with 0.01 C of charge per pulse over areas of 100 cm^2 or more.

II. APPLICATIONS

In this Section we briefly review three types of IPIB processes: surface melting and resolidification, thin film deposition, and nanophase powder synthesis. Key issues are discussed and illustrated with representative data from recent experiments on three devices: the ANACONDA[2] accelerator at Los Alamos, ETIGO[3] at Nagaoka, and TEMP[4] at Tomsk. Beam parameters are summarized in Table I. For a comprehensive bibliography on these and other applications, the reader is referred to Reference 5.

a. Rapid Melt and Solidification

Intense pulsed ion beam surface treatment (often referred to as IBEST[6]) is a thermal process that rapidly heats the surface to melt using only 10^{13}-10^{14} ions/cm^2/pulse, corresponding to an implanted species fraction of order 10^{-5} at. in the treated surface region. Typical cooling rates of this process (>10^9 K/s) are sufficient to cause amorphous layer formation and the production of non-equilibrium microstructures such as nano-crystalline and metastable phases. Experiments with lasers and low-energy electron and ion beams have shown that metal surfaces processed by a

rapid thermal quenching can have significantly improved corrosion, wear, and hardness properties. IPIB's are capable of treating a 10^2 to 10^3 cm^2 surface area in a single pulse. Protons, having ranges of 2-10 μm in most materials at typical ion energies, can provide about a 20-times deeper treatment (due to thermal diffusion, shock waves, and increased ion range) than that typical of ion implantation using heavier ions at orders of magnitude less incident energy fluence. Furthermore, pulsed rather than continuous sources allow more compact, lower-cost technology to achieve the same ion energies. Heavier ions such as nitrogen can be used to localize the energy deposition to the near-surface, inducing shock waves that propagate deeply into materials. These shocks have been reported to produce defects that significantly increase hardness and wear resistance over depths up to 100 μm.[7,8]

Steel alloys have been treated with a variety of beam energy fluences q and number of pulses N. AISI-4620 alloy (composition ≥ 96.3% wt. Fe, 0.2% C, 0.55% Mn, 1.8% Ni, 0.25% Mo, ≤ 0.04% S, ≤ 0.04% P), a common material used in gear applications, has been treated with the ANACONDA beam.[9] Processed samples have a relatively non-uniform melt zone between 0.2 and 1 μm thick, backed by a non-uniform heat-effected zone between 1 to 5-μm thick. Knoop hardness increases 1.4× to 466±30 kg/mm^2 after treatment at N = 10 and $q \approx 5$ J/cm^2. Fig. 2 shows changes in Vickers microhardness H_v of raw P18 steel (75% Fe, 0.7% C, 4% Cr, 18% W, 1% Mo, 1.2% V) after treatment at $q \approx 1.5$ J/cm^2 and N = 0, 2, 4, and 6 on the TEMP accelerator. A post-process heat treatment at 455 °C for 1 h is performed to stabilize phases and reduce point defects and dislocations. Little change in H_v is observed after this heat treatment. Processing on TEMP at $q \approx 1$ J/cm^2 of type P6M5 steel (82% Fe, 0.9% C, 4% Cr, 6% W, 5% Mo, 2% V) results in a transformation of α-Fe to γ-Fe in the near surface, a 10× increase in dislocation density, and a 100× increase in modulus. Treatment on TEMP at $q \approx 1.2$ J/cm^2 and N = 5 of type Y10A steel (> 98% Fe, 1%C, 0.25% Ni, < 0.15% W, < 0.35% Si, < 0.02% P, < 0.02%S) punches used to manufacture screwdrivers leads to considerable smoothing of the surface and to a 4.5× increase in punch lifetime.

An important feature of the rapid melt-resolidification process is surface texturing. Depending on material composition, initial surface roughness R_a, and process conditions, materials can be either roughened or smoothed. SEM and optical microscopy of 4620 steel, polished to $R_a \approx 0.1$ μm and processed on ANACONDA, reveal a smoothing over micron scale-lengths, accompanied by crater formation and large-scale (≥ 10-μm) roughening with a cellular structure similar to that observed with laser processing (Fig. 3). At N = 1 and $q \approx 5$ J/cm^2, profilometer scans indicate an increase in surface roughness to 1 μm over a ≤ 100 μm scale-length. For N = 10, roughness increases to ±2 μm, but over a coarser, 200-300 μm scale-length (Fig. 4). Qualitatively similar trends are observed at 2 J/cm^2. Comparable results are observed on tool steels processed on TEMP where R_a is of order 1 μm after treatment. Polished surfaces are roughened to this R_a while rougher surfaces are smoothed to this value.

Tungsten carbide (WC with 5% - 8% Co binder) cutting tools have been treated on TEMP. At $q \approx 1.6$ J/cm^2 and N = 1, R_a is reduced from 1.8 μm to 1.3 μm; however, R_a increases to 3 -5 μm at larger N. Improved surface-mechanical properties without roughening is achieved by a sequence of multiple pulses beginning with a single pulse at $q \approx 0.4$ J/cm^2 to pre-clean the surface, followed by a few pulses at $q \approx 0.9$ J/cm^2 to induce rapid melt and solidification, and concluding with a few pulses at 0.4 J/cm^2 to smooth the treated surface. Considerable improvements in the performance of WC drills, as evidenced by higher hole quality and tool lifetime, are observed after application of this recipe. Improved wear resistance is believed to be due to increased W solid solution in Co in the near surface. XRD and SEM analyses of T14K8 alloy (WC with 14% TiC and 8% Co) indicate that the treatment forms regions which include nanophase Co_3Ti particles with 20-30 nm grain sizes which also should improve wear resistance.

IPIB hardening of WC tools are currently a production operation, with an annual throughput of up to 100,000 pieces, by the Linetron Enterprise in N. Novgorod, Russia. The tools are constructed from T5K8 and T5K10 alloys (WC with 5% TiC with 8% and 10% Co, respectively) and are used in cutting railway wheels. The TEMP vacuum chamber is supplied with a two-axis

carrousel fixture which can accommodate 96 tools at a time (Fig. 5). Tool wear resistance is increased 2.8±0.4 times after IPIB treatment and a post-anneal.

Surface treatment of Ti- and Ni-based refractory alloys used in gas turbine blades has been studied on TEMP.[10,11] Treated surface are characterized by several distinct zones. The outer-most 0.2 to 0.4 μm of the target is ablated, leaving a residual 0.2 to 0.3 μm-thick surface with a precipitation of fine carbides and oxicarbides. The melt zone is 1 - 2 μm thick, while defects induced by the beam are observed over a 10 μm depth. After N = 100, one observes a redistribution of elements leading to decomposition and refinement of strengthening phases. Surface craters plus surface and subsurface cracks are also formed in some alloys at $q > 1$ J/cm^2. These defects are undesirable since they reduce fatigue resistance of the material. Adjusting both q and N enables one to heal these surface defects to produce a wear and corrosion resistant surface with $R_a < 0.1$ μm. Furthermore, a post-process heat treatment at 300 - 600 °C relieves residual tensile stress, anneals defects, and precipitation hardens the material. Gas corrosion resistance tests of treated turbine blades in 550-650 °C air for 100 to 500 h reveal an increase in corrosion resistance up to 10 times.[11] Long-term, full-scale tests of VT9 alloy (86% Ti, 7% Al, 3.8% Mo, 2.5% Zr, 0.35% Si, 0.25% Fe) gas turbine compressor rotor blades have been conducted with an equivalent running time of 860 h. A set of 70 blades, treated at q = 0.7-1.6 J/cm^2 and $N \geq 3$ with a post anneal of 500 °C at 2 h in $p < 10^{-6}$ Torr, was evaluated. Best results were obtained at the lowest q of 0.7 J/cm^2 where one observes a decrease in R_a from 0.24 to 0.08 μm, a reduction in oxidation layer thickness from 45 to 3 μm, and an increase in the fatigue limit from 480 to 540 MPa.[11]

b. Thin Film Deposition

In IPIB deposition, ion bombardment rapidly heats a target surface, causing vaporization and ionization (particle density up to 10^{19} cm^{-3}, electron and ion temperature of 0.2 - 2 eV, directed energy of 1 -20 eV), resulting in an ablated plume which expands outward until it is condensed as a film onto an adjacent substrate (Fig. 6).[12-15] This process is analogous to pulsed laser deposition, but uses higher total energy incident on the target allowing accelerated deposition rates or larger

area coverage. Higher beam energy densities (q = 10-50 J/cm^2) are needed for this process compared to melt and resolidification; consequently, focused beams are usually used, and heavier ion species are preferred over light species because their shorter range yields higher specific-energy deposition into a target. Advantages over conventional vapor deposition include: (1) Very high deposition rates (1 to 10 mm/s instantaneous rate) at low cost are possible; (2) Energetic ionized plume material allows the formation of materials unattainable otherwise; (3) Target material stoichiometry is preserved (congruent deposition) allowing the formation of complex films; and (4) Crucibles and filaments are eliminated improving film purity.

A variety of films including metals[14,15] (W, Ti, Mo, Nb, Au, Al, Cu, Zn), ceramics[15] (BN, SiC, $YBa_2Cu_3O_{7-x}$, ZrO_2), ZnS:Mn electroluminescent devices,[12] and $BaTiO_3$ dielectrics[16] have been prepared. Diamond-like carbon (DLC) has been deposited on ANACONDA with q = 30 J/cm^2 onto graphite targets, and 25-nm-thick films are deposited per pulse (10 mg/pulse ablated).[13] Approximately 1/3 of the ablated material is deposited on the substrates placed directly in the plume, suggesting that a substantial amount of ablated vapor does not adhere to the substrate. Framing photographs indicate that some of the plume is diverted around the substrate, possibly due to the high collisionality in the accumulated vapor. As discussed below, there are advantages in collecting this diverted vapor onto substrates positioned away from the plume line of sight.

The high instantaneous deposition rates lead to low impurity content in the film, even when deposition is performed in relatively high vacuum conditions with C, N, and O gas partial pressures of 5×10^{-5} Torr. Impurity concentrations have been measured in films deposited on TEMP from high-purity (99.99%) W and Au targets. High-purity GaAs substrates containing C, N and O concentrations of 10^{-5} % or less were used. Film thickness was inferred by X-ray fluorescence analyses. Carbon and nitrogen concentrations were determined by (d,n) nuclear reaction analysis (NRA) with 3.1 MeV deuterons. Target material surface densities σ as well as those for impurities σ_C and σ_N are shown in Table II. Background concentrations in the GaAs substrates of $\sigma_C \approx 0.8$ μg/cm^2 and $\sigma_N \approx 0.3$ μg/cm^2 have been subtracted out. Relative uncertainty of the measurements are ±10% for C and ±20% for N. While C and N are observed in W, their

concentrations in Au are below the NRA detection limit of $\sigma \leq 30\%$ of the background concentrations in the substrate. Qualitatively similar results are obtained with secondary ion mass spectrometry analyses. The carbon content f_c in W is up to an order of magnitude higher than the nitrogen content f_N. The carbon is presumably from residual gases present in the vacuum chamber since σ_C increases with the number of IPIB pulses, and since pre-sputtering of the W target before deposition does not change f_C considerably.

The angular distribution of the deposited film has been studied on TEMP with IPIB parameters of 250 A/cm^2, 9×10^7 W/cm^2, 5 J/cm^2 onto 1 cm^2 disk-shaped targets of ZnS, Nb, Au, and Pb. Film thickness varies between 0.2 and 400 nm depending on the angle θ of the substrate with respect to the target normal. The angular distribution in film thickness is highly-peaked characterized by $e^{-m\theta}$ with $3<m<4.3$ (Fig. 7). This is in contrast to the $\cos\theta$ distribution observed in conventional thermal evaporation.

Two key issues in IPIB deposition are film heating and particulate contamination. During deposition, up to 0.3 μm of material condenses in about 10 μs. The hot dense plume of plasma and neutrals plus the heat of condensation can lead to substantial transient heating of the film during deposition. Substrate heating has been confirmed on ANACONDA with thin film metal resistor substrates. Transient film temperatures up to 2000 °C are inferred for C deposition onto glass.[17]

Particulate contamination due to ablated droplets is often observed, especially when the beam power density onto the target is high.[14] Significant reduction in particulates may be obtained at the expense of reduced throughput using the "backside deposition" scheme[16] depicted in Fig. 6b. High dielectric constant, polycrystalline $BaTiO_3$ films have been prepared using this method on ETIGO with $q \approx 25$ J/cm^2. Good film morphology is observed with none of the droplets that are seen during normal front-side deposition. The deposition rates are typically 100 nm/pulse.[16]

c. Nanophase Powder Synthesis

Ultra-fine powders with nanometer-sized grains are of interest for high-density magnetic storage media, chemical catalysis, substrates for integrated circuits, and high-performance ceramics. Using a gas cloud of 1-10 Torr to supersaturate the ablated plasma formed by IPIB

vaporization of target material, powders have been synthesized on ETIGO.[18] With Al targets and O_2 gas, spherical grains of Al_2O_3 with diameters of 5 to 25 nm have been produced. At 1 Torr, nanoscale Al powder is predominate with a small γ- Al_2O_3 component, while at 10 Torr, γ- Al_2O_3 predominates with a small Al component.

Ultra-fine powders of TiO_2 and TiN have been also produced. TiO_2 particle size distributions are shown in Fig. 8 for two target - collecting mesh distances L.[19] For L = 100 mm, relatively large sizes are observed, while significantly smaller diameters are achieved at L = 330 mm. We speculate that at small L, the vapor in the plume remains too hot for condensation to occur. Large-sized grains result from vapor deposition onto the mesh. At larger L, however, there may be sufficient time for supersaturation and vapor condensation enroute between target and mesh.

III. TECHNOLOGICAL NEEDS

a. Ion Diodes

In conventional IPIB diodes, such as those used on ANACONDA and ETIGO, ions are drawn from the surface of a polymer anode[2] converted to a plasma by a combination of high-voltage flashover and electron impact. Polymer anodes are unacceptable for many materials synthesis applications because of their limited lifetime, excessive heat loading, high gas production, excessive debris, poor beam uniformity, and lack of ion species control. Several of these limitations are overcome by using an electron beam incident on a conducting anode to generate a plasma prior to the main positive polarity accelerating pulse, such as that used on TEMP.[4]

Alternately, anodes that draw ions from a performed plasma have been developed.[20] Figure 1 illustrates a plasma diode being developed for the Los Alamos CHAMP (Continuous High Average-power Microsecond Pulser) accelerator.[21] The design beam parameters are E = 200 - 250 keV, I = 15 kA, and τ = 1 μs. The diode uses a magnetically-insulated extraction diode with plasma anode in ballistically focused geometry. Focal length is adjusted by varying anode and cathode angles with respect to the system axis. The diode operates as follows. The anode consists of a flat pulsed induction coil in an aluminum housing, formed from four parallel sets of two-turn spiral windings coaxial with the system axis. The plasma anode is formed by first ducting

radially a puff of gas with a fast acting valve (risetime ~ 100 μs), located on axis, over the coil surface. When the gas puff is properly distributed, a fast rising current pulse (10 - 20 kA, 1-2 μs risetime), delivered to the induction coil breaks the gas down and induces azimuthal current in the plasma at the coil surface. The $\mathbf{j}\times\mathbf{B}$ force accelerates the plasma to the radial opening in the anode housing where it stagnates against the applied insulation magnetic field discussed below.

The cathode consists of the tips of two concentric, conical metal cylinders. The gap between the cathode tips and the plasma anode is 2 cm. Just before application of the accelerating voltage, a 200 μs risetime magnetic field B of about 0.2 T is applied transverse to the anode-cathode gap by two magnetic field coils – one located inside the inner cone and one located outside the outer cone. At peak field and when the plasma is in position at the anode housing aperture, the accelerating voltage pulse is applied to the anode. The magnitude of B is adjusted to prevent electrons from crossing the anode-cathode gap, but the more massive ions, only very weakly deflected by the B-field, are accelerated across the gap with approximately linear trajectories.

b. **Pulsed Power**

Traditional single-shot accelerators (using Marx generators and high-voltage pulse forming lines), incompatible with low-cost high-throughput commercial processing requirements, are yielding to new, short-pulse, high-average-power accelerators. The pulsed-power system definition is primarily set by the material properties of the treated product. Thermal conductivity determines pulse length, and energy required to melt or ablate and the desired per-pulse treatment area set the energy per pulse. The amount of material treated per unit time, considering material handling and treatment chamber vacuum pump-down, sets the required burst and average power levels. The desired depth of penetration, for a given ion species, and possible activation levels set the maximum allowed acceleration potential. An IPIB system has operated at 100 Hz in a 10-shot burst mode (limited by a lack of active cooling)[20] while TEMP routinely operates continuously at 0.3 Hz. Along with the development of repetitive technology, high reliability and long component and system lifetimes ($>10^8$ pulses between failure or scheduled maintenance) will have to be engineered to meet commercial needs.

Treatment of materials with high thermal conductivity requires an electrical pulse duration of less than 1 microsecond. Cooled saturable magnetic switches and inductive voltage adders, a technology developed at Sandia National Laboratories for the Ballistic Missile Defense Organization, have demonstrated continuous production of 80-ns pulses at up to 120 Hz and 300 kW.[22,23] The 10 Hz QM1 modulator shown in Fig. 9, under development at QM Technologies, is designed to deliver 24 kW average output power, at 450 kV, in 150 ns pulses to an ion diode load with a wall-plug to ion diode electrical efficiency of about 50%. This modulator uses a thyratron as the primary switch followed by 5 stages of magnetic pulse compression using 2605CO Metglas. The 2-stage linear induction adder output geometry, [23] with Metglas isolation cores, steps up the output of the pulse-forming line (PFL) to 450 kV, matches the PFL impedance to the ion diode, and allows direct access to both magnetic-insulation field coils located at dc ground potential. Two QM1 systems are now under development to obtain operational experience treating commercial parts and to establish overall system reliability.

The CHAMP electrical system design shown in Fig. 10 illustrates another path to repetitive pulsed-power technology. The pulse duration, a key system parameter is chosen from a study of overall system electrical efficiency including plasma formation and magnetic-field energy requirements, and scaling of diode performance from 1-μs pulse, single-pulse experiments. Electrical components for the diode gas valve and induction coil are housed in a "hotdeck" chassis at common potential with the pulsed anode. Solid-state switches are envisioned to deliver current from storage capacitors to the magnetic field coils at ground potential, and energy recovery techniques will be used to recover 80 to 90% of the energy delivered to the coils. The accelerating power system will utilize 4 parallel type "E" Blumlein lines each switched with by a thyratron. Blumlein lines are preferred over convention pulse lines to supply the full charge voltage into a matched load, thereby reducing by two the transformer turns ratio and the number of parallel thyratrons required. The number of networks comprising each Blumlein line will depend on the pulse fidelity required by each application. For materials processing, square voltage and current waveforms are not desired since a spread in ion energy leads to a more uniformly-distributed

energy deposition profile into the targets. Rough estimates of the electrical efficiency give (30±10)% including power to generate the anode plasma and B-field.

IV. COST ESTIMATES

Capital equipment costs for 10-kW and 30-kW IPIB systems are estimated in Table III. System specifications are: 400 kV, 1 kJ in ions/pulse, 150 ns pulsewidth, total system electrical efficiency of 23% (including the accelerator, ion beam, and vacuum systems). A surface area of approximately 200 cm^2 can be covered in a single pulse at a nominal 5 J/cm^2. Capital equipment cost estimates of \$1M and \$1.45M for 10-Hz and 30-Hz repetition rate, respectively, are dominated by the pulsed-power system (up to 2/3 of total) with the diode system and ancillaries (such as vacuum and control systems) almost equally accounting for the remainder. Materials handling equipment are not included in these estimates since they are determined by the specific application. It is interesting to compare these capital equipment costs (\$50 to \$100/Watt) with commercial pulsed laser systems which generally cost between \$500 and \$2000/Watt.

Cost-of-ownership estimates for 1- and 2-shift operation of the 10-kW system are listed in Table IV. For a capital equipment amortization period of 4 years at 8% interest and operation in a 1000 ft^2 facility at \$8/ft^2, the fixed costs are \$392K/yr. The variable costs include labor, where we assume 2 people at a burdened cost of \$55/h each, electricity at \$0.10/kW-h, and consumables of \$20/h. This gives a total cost of \$271 and \$173 per hour for 1 and 2 shift operation, respectively. These estimates may be used to predict the process cost for specific applications. This cost will depend on a number of variables, including the number of parts to be treated, their geometry, the energy level required, the number of pulses needed to do the treatment, and the cost of materials handling.

ACKNOWLEDGMENTS

This research is sponsored by the Japanese Ministry of Education, Science, Culture and Sports, the Russian State High Education Committee, and the U.S. Department of Energy.

* Present address: Varian Ion Implant Systems, 508 Dory Rd., Gloucester MA 01930.

REFERENCES

1. J. P. VanDevender and D.L. Cook, *Science* **232**, 831 (1986).
2. D. J. Rej *et. al., Rev. Sci. Instrum.* **64** (1993) p. 2753.
3. K. Yatsui *et al., Laser and Particle Beams* **3**, 119 (1985).
4. I. F. Isakov *et al., Vacuum* **42** 159 (1991).
5. H.A. Davis *et al., MRS Bulletin* **21**, 58 (1996) and references within.
6. R.W. Stinnett *et al.*, Mater. Res. Soc. Symp. **316**, 521 (1994).
7. A.D. Pogrebnjak, *Phys. Status Solidi A* **86**, 191 (1984).
8. S.A. Chistjakov, A.G. Pogrebnjak, G.E. Remnev, *Nucl. Instr. Meth. Phys. Res.* **B42** 342 (1989).
9. D.J. Rej *et al.*, submitted to *Nucl. Instr. Meth. Phys. Res. B* (1996).
10. G. E. Remnev and V. A. Shulov, *Lasers and Particle Beams* **11** 707 (1993).
11. V.A. Shulov, N.A. Nachovnaya, and G. E. Remnev, submitted to *Surf. Coat. Techn.* (1995).
12. Y. Shimotori *et. al., J. Appl. Phys.* **63** 968 (1988); K. Yatsui, *Lasers and Particle Beams* **7** 733 (1989); K. Yatsui *et al., Phys. Plasmas* **1** 1739 (1994).
13. G. P. Johnston *et. al., J. Appl. Phys.* **76** 5949 (1994).
14. C. A. Meli *et al., J. Vac. Sci. Technol.* **A13** 1182 (1995).
15. A.N. Zakoutaev *et al., Mater. Res. Soc. Symp.* **388** 388 (1995).
16. T. Sonegawa *et al., Appl. Phys. Lett.* (October 7, 1996 issue, in press).
17. J.C. Olson *et al., Mater. Res. Soc. Symp.* **388** 171 (1995).
18. K. Yatsui *et al., Appl. Phys. Lett.* **67** 1214 (1995).
19. Grigoriu *et al., Proc. Symp. Physics, Diagnostics, Applications of Pulsed High Energy Density Plasma as an Extreme State,* S. Ishii, Ed. (National Inst. Fusion Science, Nagoya, 1996) p. 25.
20. W.A. Noonan, S.C. Glidden, J.B. Greenly, D.A. Hammer, *Rev. Sci. Instr.* **66** 3448 (1995).
21. H.A. Davis *et al., Rev. Sci. Instrum.* (Jan. 1997, in press).
22. E.L. Neau *et al.*, submitted to *Nucl. Instr. Meth. Phys. Res. B (1996).*
23. H.C. Harjes *et. al., Proc of the 8th IEEE Int'l Pulsed Power Conf.*, R. White and K. Prestwich, eds. (IEEE, Piscataway NJ, 1992) p.543.

TABLE I

Intense pulsed ion beam accelerator parameters.

Device	E (keV)	I (kA)	τ (ns)	Species	Repetition Rate
ANACONDA[2]	350	30	1000	H, C, O	1 pulse / 3min
ETIGO[3]	1000	60	70	H, C	1 pulse / 5 min
TEMP[4]	300	20	50	C	0.3 Hz

TABLE II

Film surface densities and concentrations of target material, and carbon and nitrogen impurities obtained on TEMP with tungsten and gold targets.

Target	No. pulses	σ (mg/cm^2)	σ_C ($\mu g/cm^2$)	f_C (% wt)	σ_N ($\mu g/cm^2$)	f_N (% wt)
W	30[a]	0.45	2.3	0.51	0.77	0.17
W	100[b]	1.1	11.8	1.1	0.97	0.09
W	100[c]	1.3	9.7	0.75	0.62	0.05
Au	5[b]	0.2	< 0.2	< 0.1	< 0.1	< 0.05

[a] without pre-deposition sputtering of target surface and without a LN_2 cold trap.

[b] with pre-deposition sputtering and without a LN_2 cold trap.

[c] with pre-deposition sputtering and with a LN_2 cold trap.

TABLE III

Capital equipment costs (in $K) for 10-kW and 30-kW average power systems.

Hardware	10-kW System	30-kW System
Pulsed Power	650	850
Ion Diode (incl. plasma anode)	150	300
Vacuum and controls	200	300
TOTAL	**1000**	**1450**

TABLE IV

Cost of ownership ($/h) for a 10-kW IPIB system for 1-shift (2000 h/yr) and 2-shift (4000 h/yr) operations.

Item	1-shift	2-shift
Capital amortization	$192	$96
Space	4	2
Labor	55	55
Electricity	5	5
Consumables	15	15
TOTAL	**$271**	**$173**

FIGURE CAPTIONS

1. Magnetically-insulated intense pulsed ion beam (IPIB) diode.

2. Vickers hardness *vs* indenter depth of P18 steel processed on the TEMP IPIB accelerator.

3. Optical micrographs of AISI-4620 steel processed at $q \approx 5$ J/cm^{2}on the ANACONDA IPIB accelerator.

4. Surface dimensions of 4620 steel processed on the ANACONDA IPIB measured with a 25-μm-diam profilometer stylus.

5. (a) Schematic diagram of the TEMP carrousel (1) and IPIB diode (2); (b) Photograph of TEMP showing WC(Co) tools, used to cut railway wheels, mounted on the carrousel.

6. Schematic of IPIB thin film deposition for the (a) front and (b) backside configurations.

7. (a) Schematic depicting the angular distribution measurements; (b) angular distributions of deposited films $F(\theta)/F(0) = \exp\{-m\theta\}$ with m = 3.1 for Nb, 3.4 for Pb, 3.0 for ZnS, and 4.3 for Au on TEMP.

8. Distribution of particle sizes for TiO_2 formed on the ETIGO accelerator with target-collecting mesh separations L of (a) 100 mm and (b) 330 mm. (from Ref. 19).

9. The 10 Hz QM1 modulator designed to deliver 24-kW average output power at 450 kV to an ion diode load: 1) 2 stage induction adder, 2) 150 ns pulse forming network, 3) intermediate energy store, 4) controls and diagnostics, 5) oil purification and transfer system, and 6) water deionization and transfer system

10. Repetitive pulsed power circuit for the CHAMP accelerator under construction at Los Alamos.

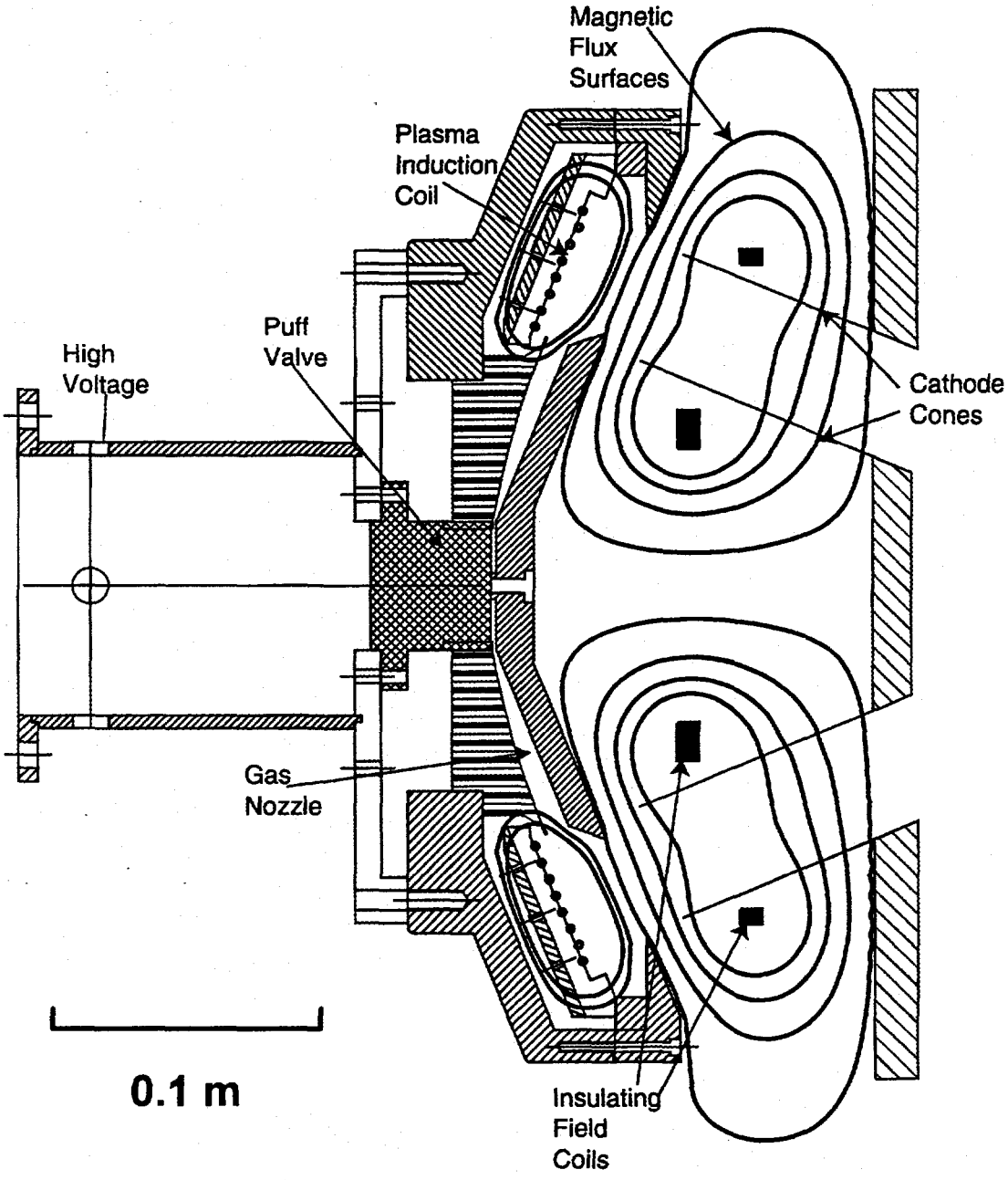
Magnetic
Flux
Surfaces
Plasma
Induction
Coil
Puff
Valve
High
Voltage
Cathode
Cones
Gas
Nozzle
0.1 m
Insulating
Field
Coils

Fig. 1

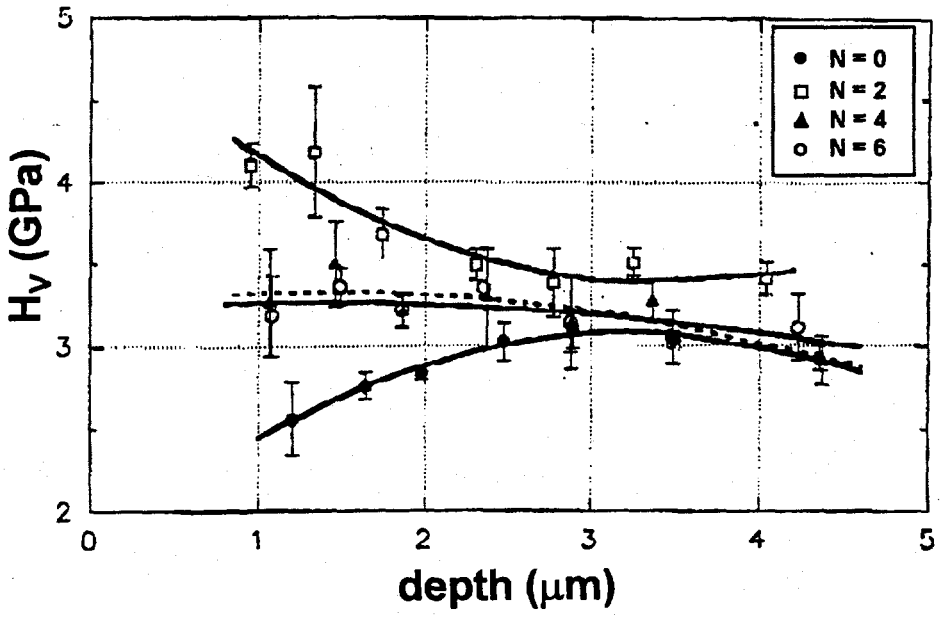

Fig. 2

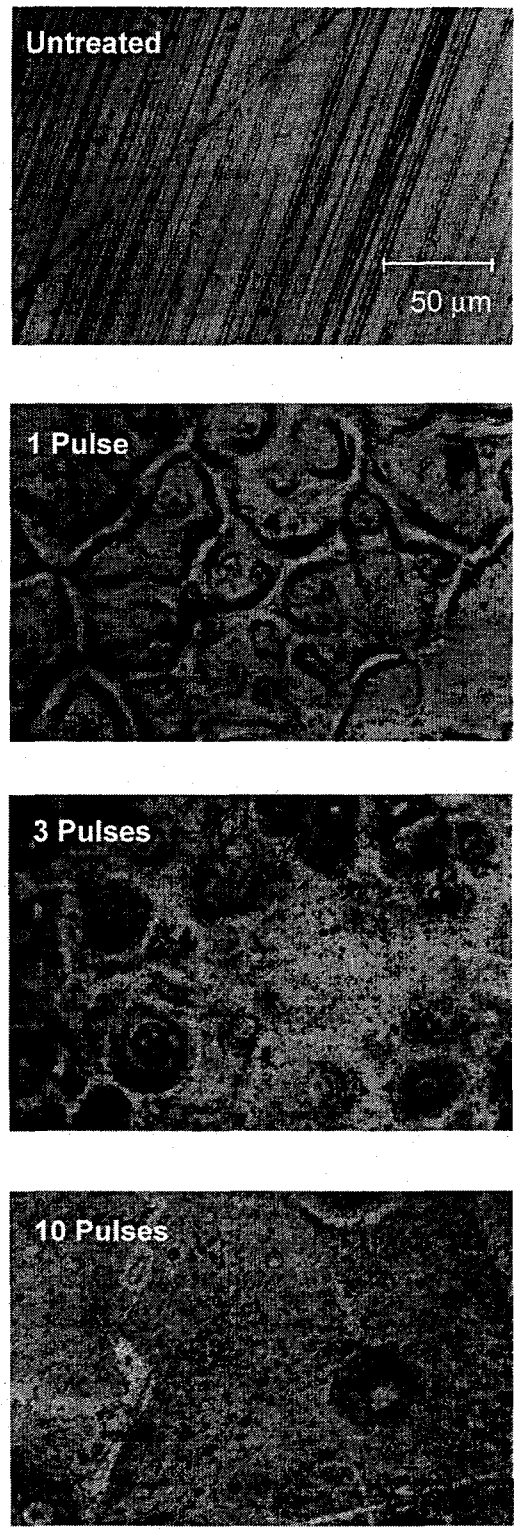

Fig. 3

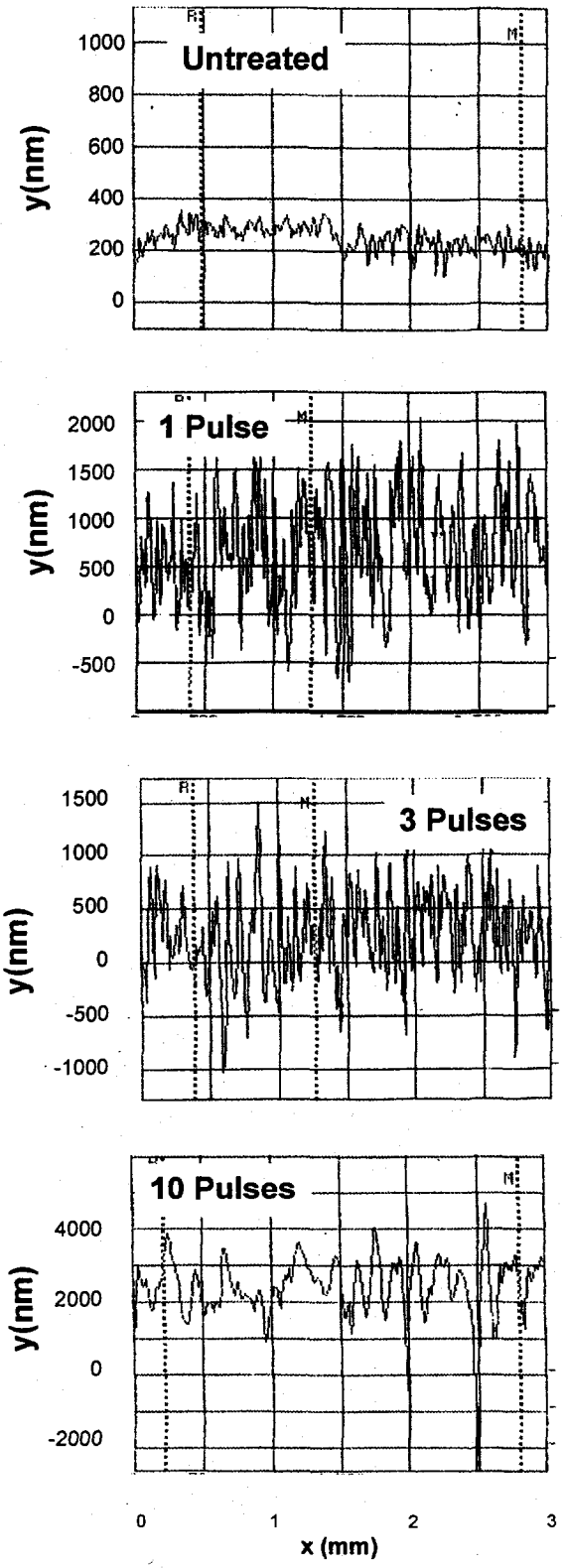
Untreated
1 Pulse
3 Pulses
10 Pulses
y(nm)
x (mm)
1000
800
600
400
200
0
2000
1500
1000
500
0
-500
1500
1000
500
0
-500
-1000
4000
2000
0
-2000
0
1
2
3

Fig. 4

(a)

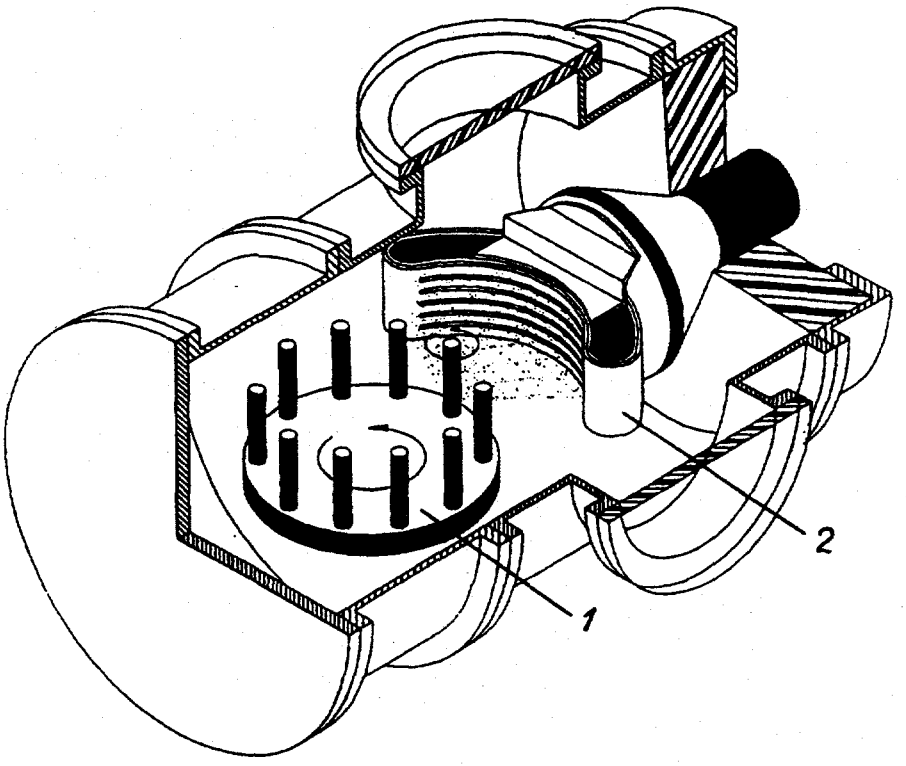

(b)

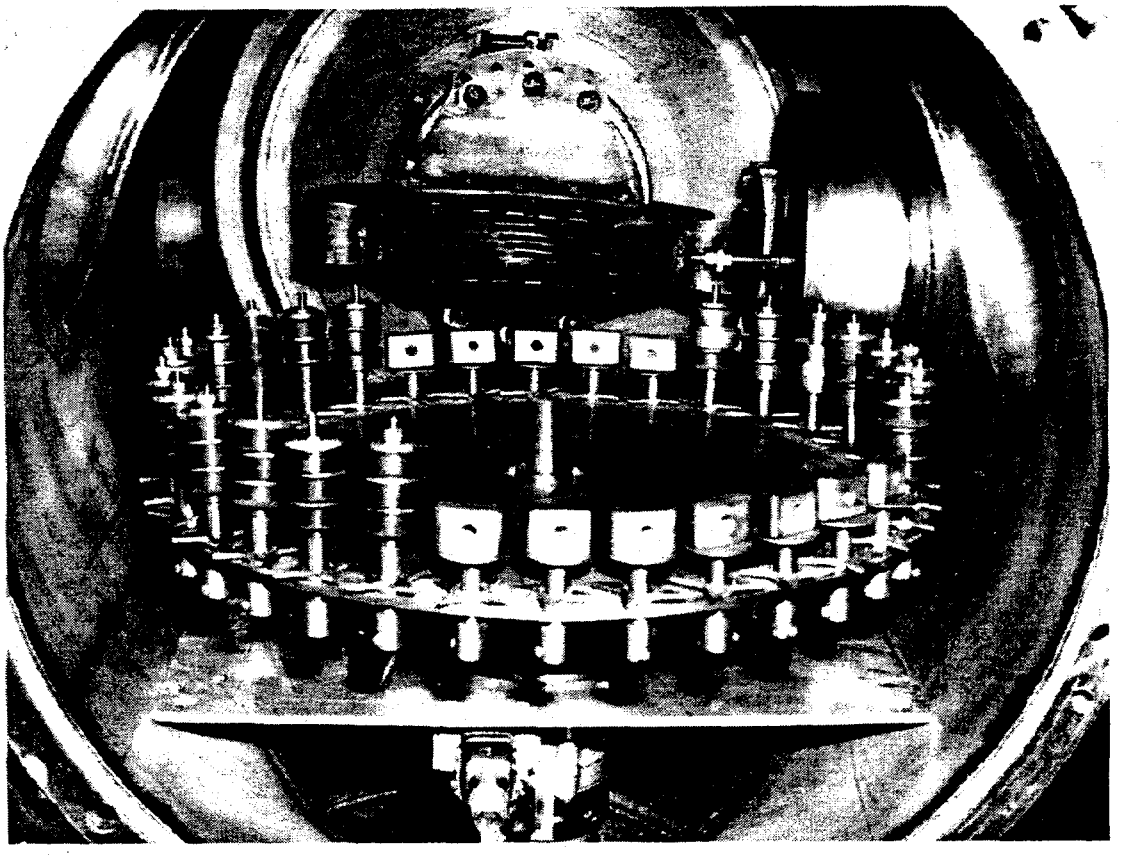

Fig. 5

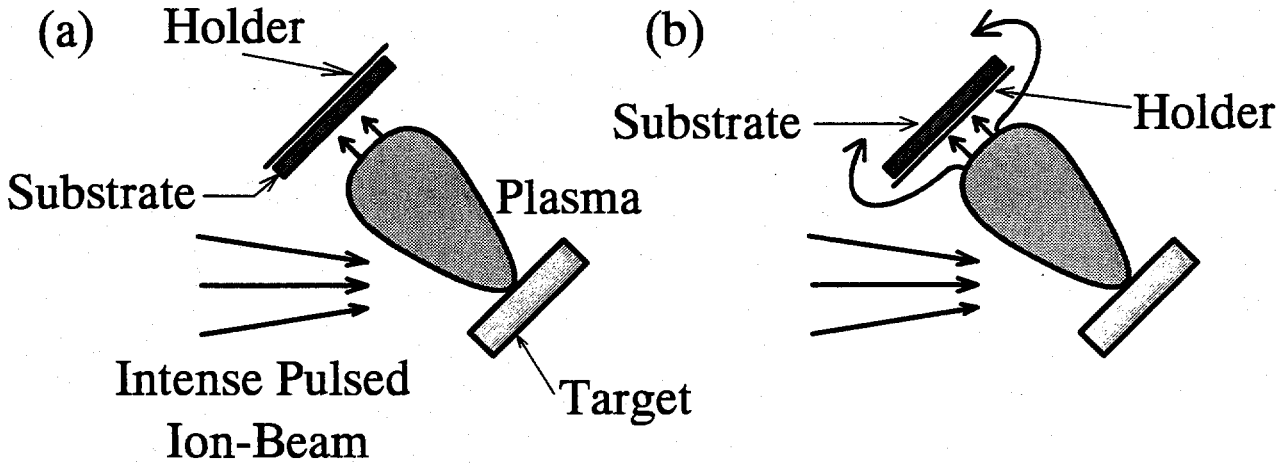
(a)
Holder
Substrate
Plasma
Intense Pulsed
Ion-Beam
Target
(b)
Substrate
Holder

Figure 6

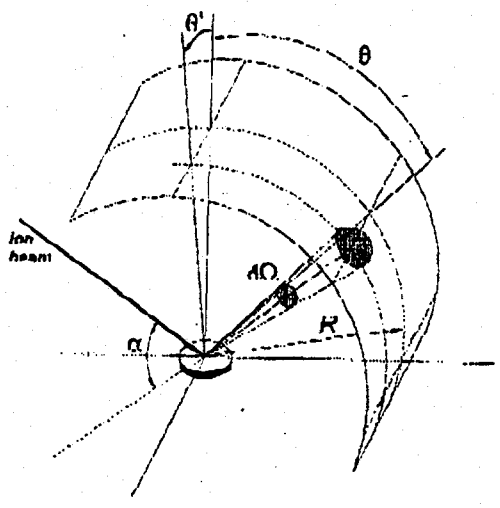
θ'
θ
ion beam
dΩ
R
α

(a)

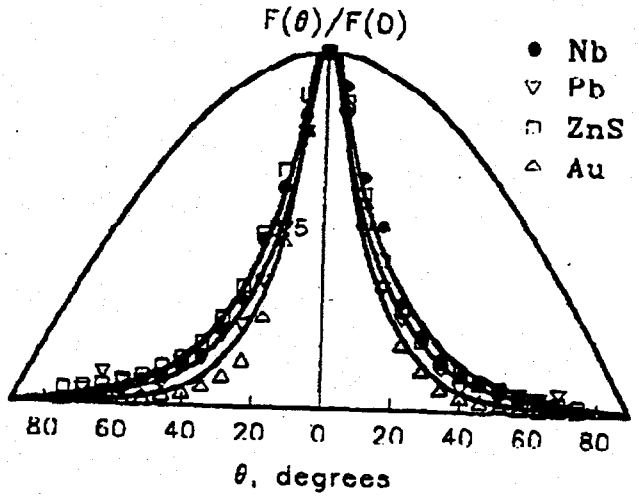
F(θ)/F(0)
Nb
Pb
ZnS
Au
80 60 40 20 0 20 40 60 80
θ, degrees

(b)

Fig. 7

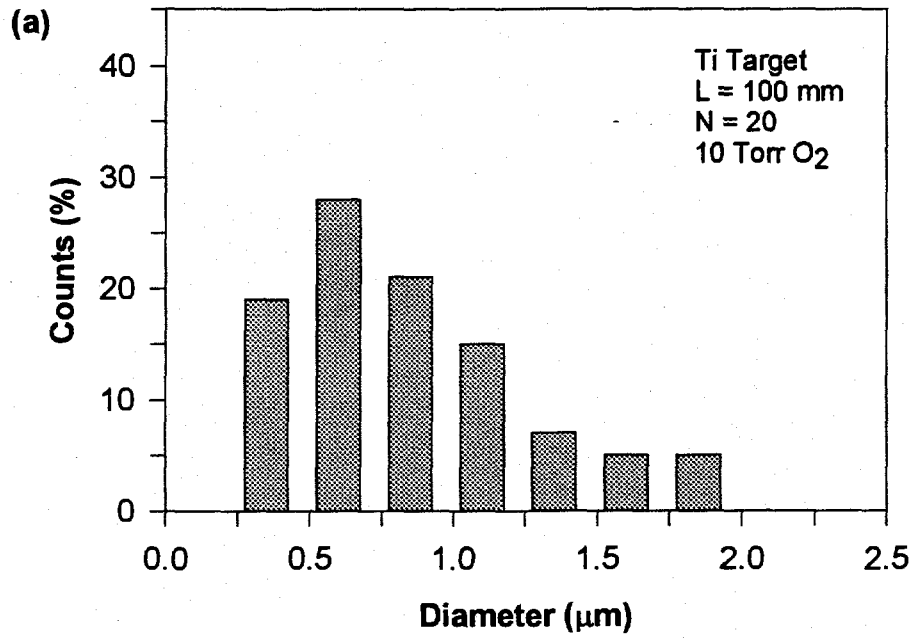
(a)
Ti Target
L = 100 mm
N = 20
10 Torr O_2
Counts (%)
0
10
20
30
40
0.0
0.5
1.0
1.5
2.0
2.5
Diameter (μm)

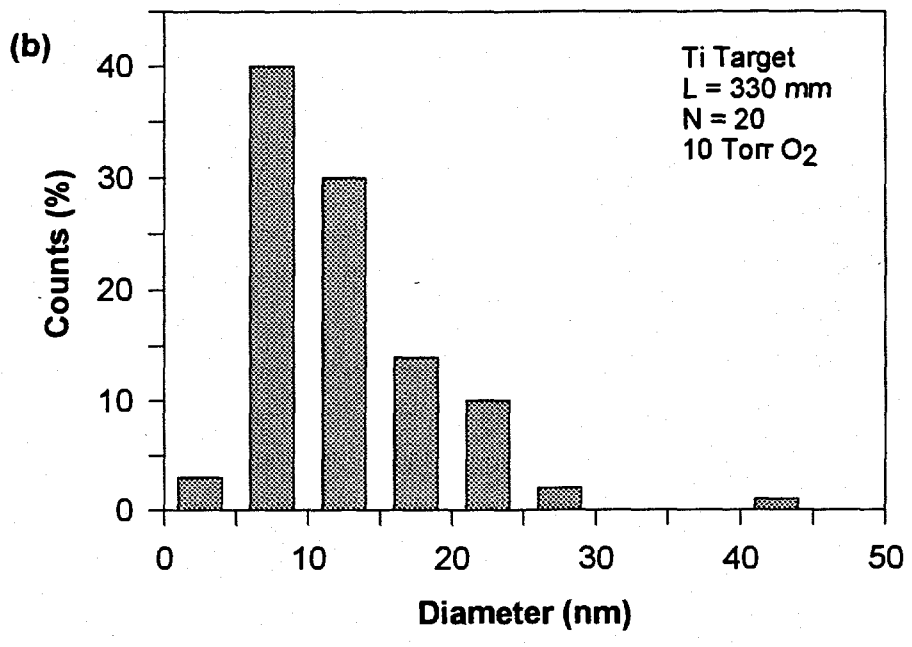
(b)
Ti Target
L = 330 mm
N = 20
10 Torr O_2
Counts (%)
0
10
20
30
40
0
10
20
30
40
50
Diameter (nm)

Fig. 8

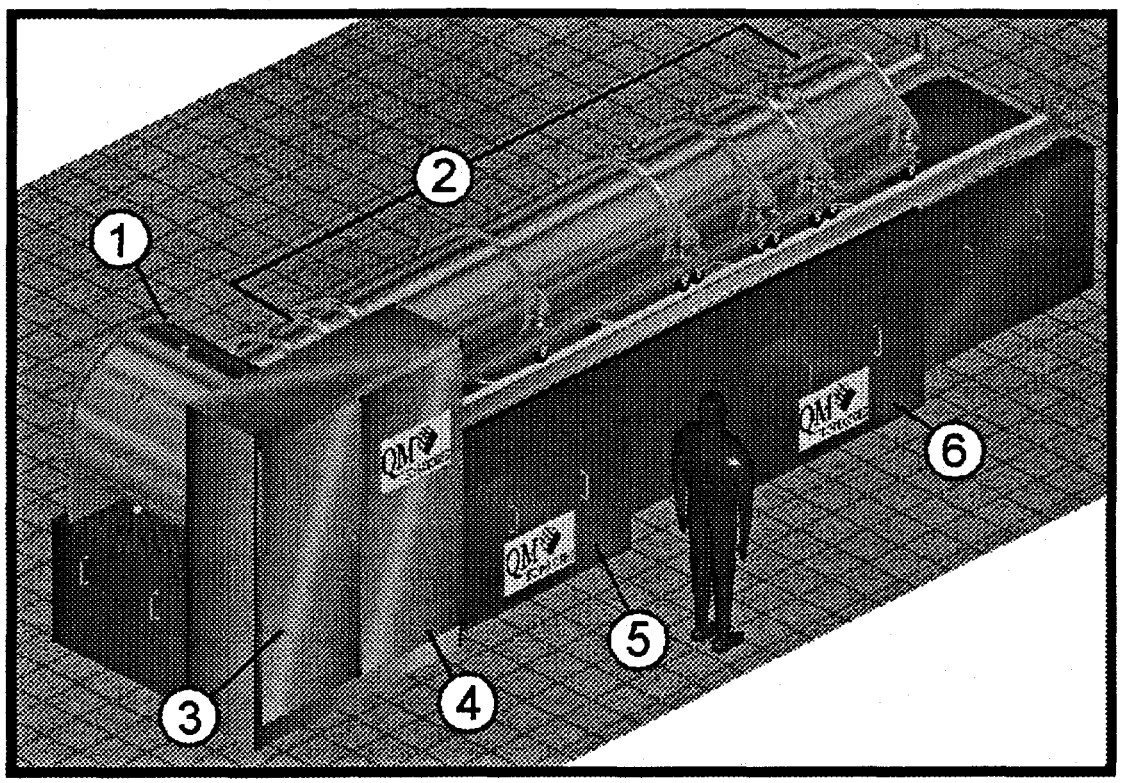

Fig. 9

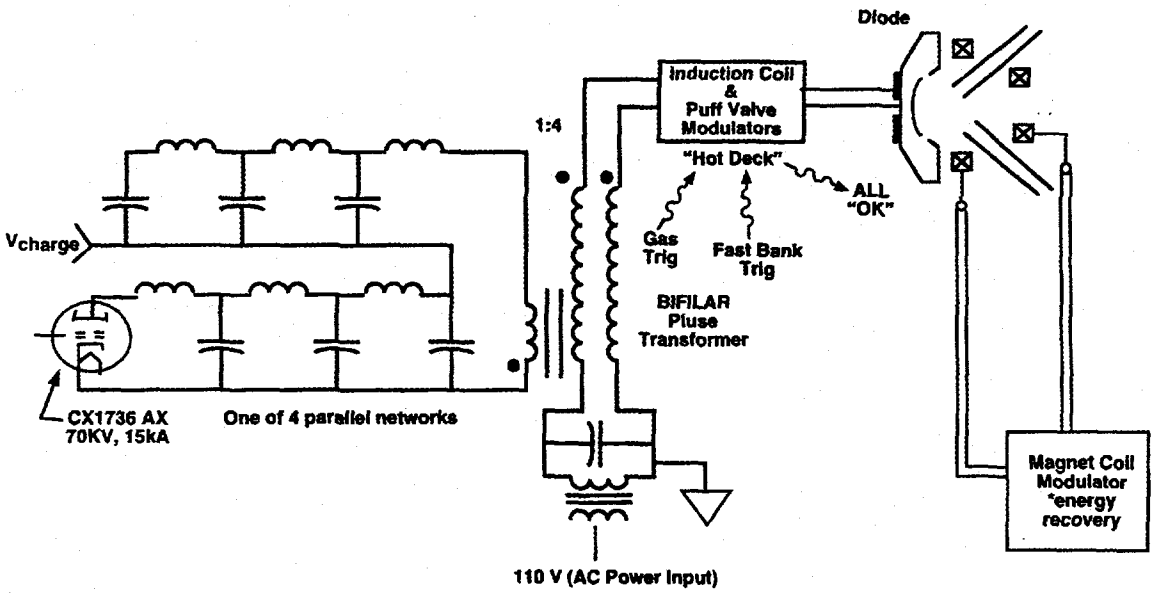
Diode
Induction Coil
&
Puff Valve
Modulators
1:4
"Hot Deck"
ALL
"OK"
Gas
Trig
Fast Bank
Trig
BIFILAR
Pluse
Transformer
Vcharge
CX1736 AX
70KV, 15kA
One of 4 parallel networks
Magnet Coil
Modulator
*energy
recovery
110 V (AC Power Input)

Fig. 10